Short communication

Three-dimensional hemisphere-structured LiSn$_{0.0125}$Mn$_{1.975}$O$_4$ thin-film cathodes

CrossMark

Haena Yim [a,d], Woo Yeon Kong [a,b], Seok-Jin Yoon [a], Sahn Nahm [b], Ho Won Jang [c], Yung-Eun Sung [d,e], Jong-Yoon Ha [f], Albert V. Davydov [f], Ji-Won Choi [a,*]

[a] Electronic Materials Research Center, Korea Institute of Science and Technology, Seoul 136-791, Republic of Korea
[b] Department of Materials Science and Engineering, Korea University, Seoul 136-701, Republic of Korea
[c] Department of Materials Science and Engineering, Research Institute of Advanced Materials, Seoul National University, Seoul 151-744, Republic of Korea
[d] School of Chemical and Biological Engineering, Seoul National University, Seoul 151-744, Republic of Korea
[e] Center for Nanoparticle Research, Institute for Basic Science (IBS), Seoul 151-742, Republic of Korea
[f] Materials Science Engineering Division, National Institute of Standards and Technology, Gaithersburg, MD 20899, USA

ARTICLE INFO

ABSTRACT

Three-dimensional (3D) high surface area LiSn$_{0.0125}$Mn$_{1.975}$O$_4$ thin film cathodes have been fabricated in order to increase a charge capacity in the Li-ion battery. Metal oxide films were deposited by RF magnetron sputtering on three types of hemisphere-structured templates fabricated via spin-coating with polystyrene (PS) beads. Compared to standard planar battery design, the capacities of the close-packed, linked, and isolated 3D films are higher by 1.4, 2.6, and 2.1 times, respectively, which correlates with the corresponding increase of the specific surface area of the templates. The linked hemisphere cathode film shows an improved discharge capacity of 67.6 µA h µm^{-1} cm^{-2} without significant degradation of the cyclic retention.

1. Introduction

One of the promising cathode materials in Li-ion batteries is LiMn$_2$O$_4$ due to its ability to operate at a high cell voltage, low toxicity, and low cost. However, the major problem is a gradual capacity loss resulting from the "Jahn–Teller distortion" accompanied by a drop in the average valence state of Mn below 3.54 V [1]. To suppress capacity fading, substitutions of the Mn^{3+} ions with other cations, such as Fe^{2+}, Ni^{2+}, and Co^{2+} [2], have been studied because of providing increased valence of the Mn ion. The electrochemical properties of Sn-substituted LiSn$_{x/2}$Mn$_{2-x}$O$_4$ thin films, which have high capacity retention without the initial capacity loss, make them suitable as cathode materials [3].

In addition to optimizing cathode material, the demands for miniaturized thin-film batteries for electronic devices like RFID tags, MEMS, and smart-card devices are steadily increasing. Thin-film batteries with a small footprint area have a high energy density, good rechargeability, no memory effect, and applicability to flexible devices. However, the 2D thin-film battery designs are reaching their limit. For example, increasing the thickness of the cathode has no significant effect on the efficiency of the electrochemically active area at the cathode/electrolyte(C/E) interface. On the contrary, in a 3D thin-film battery design, it is expected that ionic conductivity will scale up because of a shorter path for the Li

ions at the C/E interface with the cathode thickness due to the increased electrochemically active area. Thus, developing 3D electrode architecture with increased surface area and good ionic conductivity shows a promise in facilitating high capacity and fast Li ion mobility in the battery [4]. Several examples of 3D electrode thin films have been presented. For example, Gowda et al. reported the nanowire architecture thin film [5], and Baggetto et al. reported the trench structured film, and these films shows increased discharge capacity [6]. Also, Notten et al. published uniformly integrated 3D all-solid-state batteries by using solid-electrolyte LiPON which can provide more stable electrochemical performances because of its thermal stability [7]. However, these 3D electrodes often require a complicated, multi-step processing entailed with a high cost. In this work, the hemisphere-structured LiSn$_{0.0125}$Mn$_{1.975}$O$_4$ thin film cathodes were fabricated on close-packed, linked, and isolated polystyrene (PS) bead templates through a one-step spin-coating process, which provides a fast and easy process to fabricate the 3D structure, followed by an investigation of their microstructure and discharge capacity.

2. Material and methods

2.1. Preparation of hemisphere-structured films

A suspension of 700 nm diameter polystyrene (PS) beads was spin-coated onto a SiO$_2$/Si substrate. Prior to the spin-coating, the SiO$_2$/Si substrate was treated with oxygen plasma at 150 W, using a microwave plasma etcher (PINK, Wertheim-Bestenheid, Germany) to obtain a

* Corresponding author at: 136-791, KIST, 14-gil 5, Hwarangno, Seongbuk-gu, Seoul 136-791, Korea. Tel.: +82 2 958 5556.
E-mail address: jwchoi@kist.re.kr (J.-W. Choi).

hydrophilic surface to assist in the close-packing of PS layers. After the treatment, a drop of PS suspension was spin-coated on the substrate at 1100 rpm for 3 s and dried for 1 h at room temperature, which resulted in a closed-packed monolayer on the template. Oxygen plasma etching at 90 W RF power and 20 s to 70 s duration was carried out to fabricate linked and isolated PS bids templates. Oxygen plasma etching for 20 s caused the PS microspheres to reduce their size and form "bridges" (the samples with such "bridges" are referred to as the "linked templates"). Upon further oxygen plasma exposure, the "bridges" got etched away, thus leading to complete isolation of the PS microspheres, dubbed as "isolated templates". Following oxygen plasma treatment, 50 nm Ti was deposited onto the templates followed by 100 nm Pt. The metal coated substrate was annealed in air at 500 °C for 30 min to burn out the PS bead organic material. Then, the ≈ 150 nm thick $LiSn_{0.0125}Mn_{1.975}O_4$ cathode material was deposited via RF sputtering on the obtained 3D structured templates. Finally, the samples were annealed in oxygen at 500 °C for 2 h to obtain fully crystallized oxide films.

2.2. Structural characterization

The surface morphology of the samples was analyzed using a field emission scanning electron microscope (FESEM), XL-30 (FEI, USA). The phase identification of the thin film was carried out with an X-ray diffractometer (XRD) (D/Max-2500 (Rigaku, USA)), using Cu Kα radiation. Transmission electron microscope (TEM) Titan 80-300 (FEI, USA) and selected-area electron diffraction (SAED) were used to analyze oxide film microstructure. Half-type cells were assembled to evaluate the electrochemical properties of the hemisphere-structured oxide cathodes, utilizing a lithium foil anode in a 1 M solution of $LiPF_6$ in a 1:1 vol.% mixture of ethylene carbonate (EC) and diethyl carbonate (DEC). The cells were tested in an argon filled glove box by WBCS3000 (WonATech, South Korea).

3. Results and discussion

The microstructure of $LiSn_{0.0125}Mn_{1.975}O_4$ films deposited on the templates followed by annealing at 500 °C was examined by the XRD and TEM. Fig. 1(a) shows $\Omega - 2\Theta$ scans for the planar and hemisphere morphologies. Both films were confirmed to have a spinel structure (Fd-3 m; PDF#89-011820) with the lattice parameter values, a = 8.220(3) Å and a = 8.233(1) Å, respectively, in agreement with literature data for $LiMn_2O_4$ [8]. Corresponding TEM images are shown in Fig. 1(b) and (e). The thickness of the $LiSn_{0.0125}Mn_{1.975}O_4$ thin films was ~150 nm, indicating that the rate and uniformity of the thin film
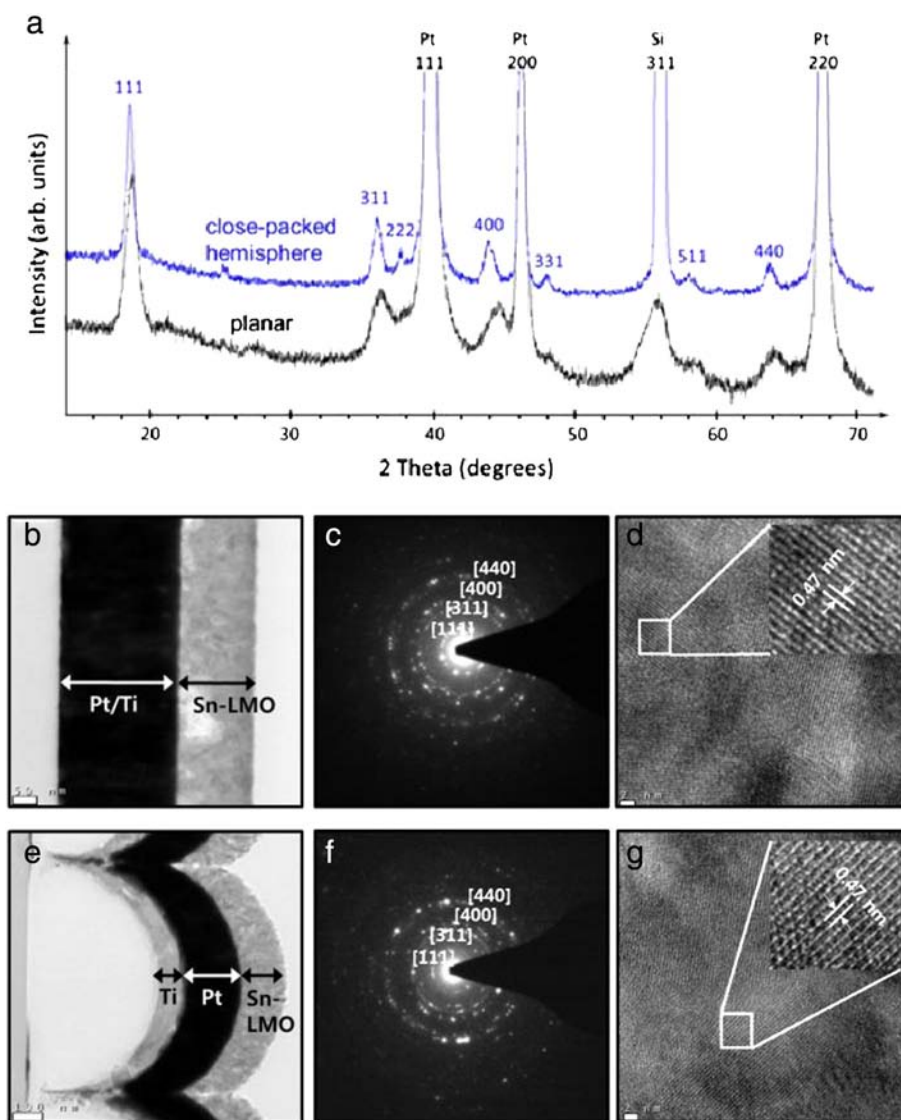
Fig. 1. (a) XRD $\Omega - 2\Theta$ scans for the $LiSn_{0.0125}Mn_{1.975}O_4$ planar and close-packed hemisphere type thin films. (b–d) cross-section TEM image, corresponding SAED pattern and HRTEM image of the planar film; (e–g) cross-section TEM image, corresponding SAED pattern and HRTEM image of the close-packed hemisphere type film.

deposition were unaffected by the device geometry. The SAED patterns in Fig. 1(c) and (f) confirm that the $LiSn_{0.0125}Mn_{1.975}O_4$ films are polycrystalline. The 0.47 nm d-spacing of the lattice fringes in high-resolution TEM images [Fig. 1(d) and (g)] corresponds to the [111] plane of $LiMn_2O_4$ spinel structure. These results indicate that the PS bead induced morphology had no adverse effect on the crystallinity of the film.

The hexagonal close-packed PS monolayer template was manufactured via facile and scalable spin-coating process. Oxygen plasma etch resulted in shrinkage of PS beads with the formation of residual "bridges", while longer plasma exposure resulted in the complete separation of PS microspheres. Cross-sectional SEM images in Fig. 2 confirmed homogeneous conformal oxide deposition for the planar, close-packed hemisphere, linked hemisphere, and isolated hemisphere (a–d) geometries. The corresponding surface areas of the thin films were calculated for cases (a) to (d) as outlined by red dotted lines in Fig. 2. The limited square area, which includes six spheres for convenient calculation, was considered, and the active surface area of each sphere was calculated using the spherical cap formula. The effective oxide surface areas of the close-packed, linked, and isolated hemispheres were, respectively, 1.3, 2.6, and 2.1 times larger compared to the planar film surface area. Fig. 3(a) shows the second cycled voltage-capacity profiles of planar surface design vs. linked hemisphere-structured $LiSn_{0.0125}Mn_{1.975}O_4$ film within the potential range of 3.0–4.3 V at a 1 C rate. There are two plateaus for the charge and discharge profiles for both samples: a plateau at 4.00 V corresponds to the $LiMn_2O_4$/ $Li_{0.5}Mn_2O_4$ transformation, and a plateau at 4.15 V to the $Li_{0.5}Mn_2O_4$/ λ-Mn_2O_4 transformation [9]. A small number of charges are stored between 3.6 and 3.8 V, which correspond to removing oxygen vacancies in the lattice [10]. The charge capacities are 30 and 115 μA h μm^{-1} cm^{-2} for planar and linked hemisphere structures in Fig. 3(a), respectively. Also, the discharge capacities are 25.7 and 67 μA h μm^{-1} cm^{-2} for planar and linked hemisphere structures. The worse coulombic efficiency of the linked-hemisphere film than that of the planar film can be explained by the larger surface area leading to more irreversible reactions such as SEI formation.

The discharge capacities of the planar and hemisphere-structured films were measured as shown in Fig. 3(b). The planar film had an initial capacity of 25.7 μA h μm^{-1} cm^{-2}, while the initial capacities

of close-packed, linked and isolated hemisphere-shaped films were 35.3 μA h μm^{-1} cm^{-2}, 67 μA h μm^{-1} cm^{-2}, and 59 μA h μm^{-1} cm^{-2}, respectively. Noticeably, they were 1.4, 2.6, and 2.1 times higher than that of the planar film, thus scaling linearly with the corresponding cathode surface areas in Fig. 3(c). The discharge capacity of 3D structured samples has also improved compared to the planar film: the linked film possessed 2.23 times higher discharge capacity after 100 cycles than planar film. The capacity retention at 100 cycles was comparable for the 3D vs. planar geometries: planar films, close-packed, linked, and isolated hemisphere samples yielded 71%, 66%, 61% and 62% retention ratios, respectively. The capacity retentions are stabilized to 89%, 84%, 76% and 75% after 30 cycles. The electrochemical reason of improved cyclability of $LiSn_{0.0125}Mn_{1.975}O_4$ cathode thin film has been reported through preceding research by XPS and NEXAFS study [3]. The analysis indicated that the average valence state of Mn could be increased over 3.54 V, which leads to suppression of Jahn–Teller distortion effects.

A reason for the slight decrease of the retention efficiency in 3D-structured films could be associated with the less robust performance of the platinum electrode compared to that for the planar geometry. Unlike the planar case, where the Pt electrode is a continuous thick layer, the Pt interconnects between the hemispheres, especially for the linked and isolated geometries could be much thinner due to the shadowing effects during metal deposition (see potential "weak" spots marked by the blue circles in Fig. 2(c) and (d)). These thin Pt "bridges" might degrade mechanically during cycling due to electromigration enhanced by possible Joule-heating effect. For the same reason, the Pt current collector beneath the cathode film can also be thin in some regions (note that the inner parts of platinum electrodes are hollow [11]). Thus, the $LiSn_{0.0125}Mn_{1.975}O_4$/Pt structures adjacent to the valley regions between the hemispheres could get disconnected during the cycling test, causing a slight decrease in the cathode retention performance.

4. Conclusion

In summary, all three types of hemisphere thin films showed a higher discharge capacity than the planar film. The linked hemisphere-structured film exhibited the best discharge capacity of 67 μA h μm^{-1} cm^{-2}, which is 2.6 times higher than that of the planar

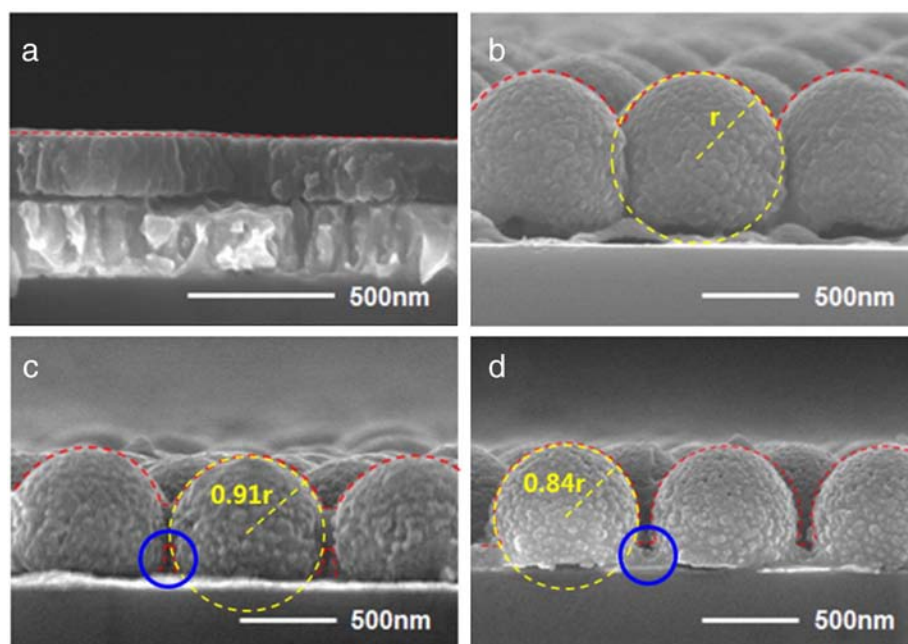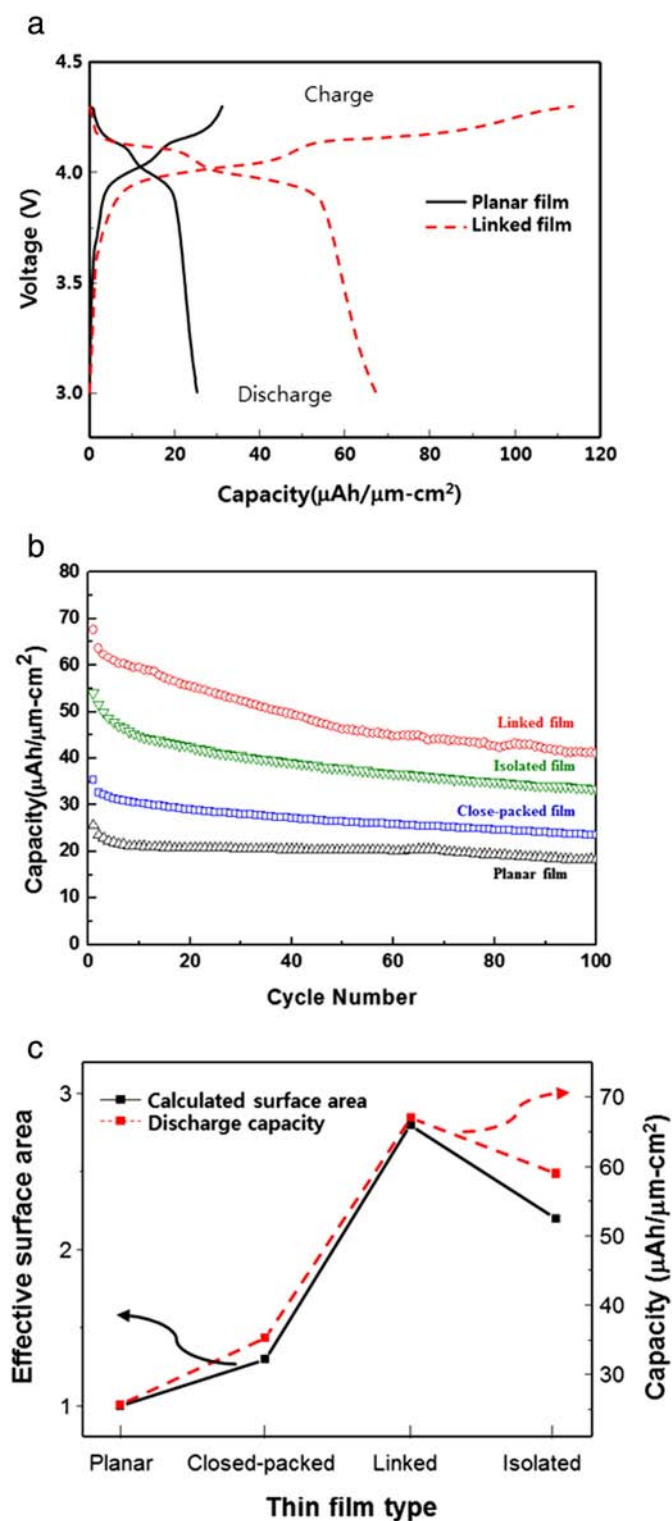**Fig. 2.** SEM images of the $LiSn_{0.0125}Mn_{1.975}O_4$ cathode thin films: (a) planar films; (b) close-packed films; (c) linked films; and (d) isolated films.

Fig. 3. (a) Voltage profile for the planar and linked hemisphere-structured LiSn$_{0.0125}$Mn$_{1.975}$O$_4$ thin films, (b) discharge capacity as a function of cycling for the planar, close-packed, linked, and isolated hemisphere-structured thin films, and (c) the correspondence between the effective surface area and discharge capacity.

film and is proportional to the effective surface area increase. Due to its improved discharge capacity and facile fabrication process, the hemisphere-structured LiSn$_{0.0125}$Mn$_{1.975}$O$_4$ film has potential applications in all-solid-state thin-film batteries.

Acknowledgement

References

[1] C.Y. Ouyang, S.Q. Shi, M.S. Lei, J. Alloy Compd. 474 (2009) 370.
[2] S.Q. Shi, C.Y. Ouyang, D.S. Wang, L.Q. Chen, X.J. Huang, Solid State Commun. 126 (2003) 531.
[3] D.W. Shin, J.W. Choi, W.K. Choi, Y.S. Cho, S.J. Yoon, Electrochem. Commun. 11 (2009) 695.
[4] M.H. Park, K. Kim, J. Kim, J. Cho, Adv. Mater. 22 (2010) 415.
[5] S.R. Gowda, A.L.M. Reddy, X.B. Zhan, H.R. Jafry, P.M. Ajayan, Nano Lett. 12 (2012) 1198.
[6] L. Baggetto, H.C.M. Knoops, R.A.H. Niessen, W.M.M. Kessels, P.H.L. Notten, J. Mater. Chem. 20 (2010) 3703.
[7] P.H.L. Notten, F. Roozeboom, R.A.H. Niessen, L. Baggetto, Adv. Mater. 19 (2007) 4564.
[8] I. Yamada, T. Abe, Y. Iriyama, Z. Ogumi, Electrochem. Commun. 5 (2003) 502.
[9] D.K. Kim, P. Muralidharan, H.W. Lee, R. Ruffo, Y. Yang, C.K. Chan, H. Peng, R.A. Huggins, Y. Cui, Nano Lett. 8 (2008) 3948.
[10] W. Liu, K. Kowal, G.C. Farrington, J. Electrochem. Soc. 145 (1998) 459.
[11] H.G. Moon, Y.S. Shim, H.W. Jang, J.S. Kim, K.J. Choi, C.Y. Kang, J.W. Choi, H.H. Park, S.J. Yoon, Sensors Actuators B Chem. 149 (2010) 116.